

Information about the correction:

Figure 8 was improper in the original PDF version of this article, published on April 1, 2022. This has been corrected in the PDF version of the article on October 19, 2022. The other elements of the article remain unchanged.

Alagani HARISH ¹, Vasudevan RAGHAVAN ¹

Numerical study of laminar non-premixed biogas-air flames behind backward facing steps

Received 18 October 2021, Revised 5 January 2022, Accepted 7 January 2022, Published online 1 April 2022

Keywords: biogas, non-premixed flames, backward facing step, flame stability, detailed kinetics

Biogas, a renewable fuel, has low operational stability range in burners due to its inherent carbon-dioxide content. In cross-flow configuration, biogas is injected from a horizontal injector and air is supplied in an orthogonal direction to the fuel flow. To increase the stable operating regime, backward facing steps are used. Systematic numerical simulations of these flames are reported here. The comprehensive numerical model incorporates a chemical kinetic mechanism having 25 species and 121 elementary reactions, multicomponent diffusion, variable thermo-physical properties, and optically thin approximation based volumetric radiation model. The model is able to predict different stable flame types formed behind the step under different air and fuel flow rates, comparable to experimental predictions. Predicted flow, species, and temperature fields in the flames within the stable operating regime, revealing their anchoring positions relative to the rear face of the backward facing step, which are difficult to be measured experimentally, have been presented in detail. Resultant flow field behind a backward facing step under chemically reactive condition is compared against the flow fields under isothermal and non-reactive conditions to reveal the significant change the chemical reaction produces. Effects of step height and step location relative to the fuel injector are also presented.

1. Introduction

Biogas is produced due to anerobic fermentation of organic materials such as cow dung, animal and food wastes [1, 2]. Composition of biogas varies based on the source used for its production. Biogas mainly contains methane and carbon dioxide, where the volumetric proportion of carbon-dioxide varies in the range of 15%–60%

✉ Vasudevan Raghavan, e-mail: raghavan@iitm.ac.in

¹Indian Institute of Technology Madras, Chennai, India. ORCID: A.H. 0000-0001-9523-6478, V.R. 0000-0002-6480-613X



© 2022. The Author(s). This is an open-access article distributed under the terms of the Creative Commons Attribution-NonCommercial-NoDerivatives License (CC BY-NC-ND 4.0, <https://creativecommons.org/licenses/by-nc-nd/4.0/>), which permits use, distribution, and reproduction in any medium, provided that the Article is properly cited, the use is non-commercial, and no modifications or adaptations are made.

based on the raw material and method of its production [3–7]. During combustion, presence of carbon-dioxide imparts both positive and negative effects on the flame characteristics. The negative aspect is due to the thermal absorption characteristics of carbon-dioxide and its inert nature. The positive aspect is that the carbon-dioxide helps in reducing emissions of nitric oxides. In flames using methane and carbon-dioxide mixture, as the percent of carbon-dioxide was increased, the heat release rate decreased and the flame stability was affected [8–10]. Due to a decrease in the heat release rate, the flame temperature reduced [11, 12] and as a result, the laminar burning velocity also decreased [11–13]. On the positive aspect of carbon-dioxide, due to the reduction in flame temperature, nitric oxides emissions decreased [11, 14–16]. The soot formation was also found to be suppressed by the addition of carbon-dioxide [17].

Since the presence of carbon-dioxide in the fuel mixture causes a reduction in the calorific value, for a given power rating of the burner, higher mass flow rate of the fuel mixture is required. Instabilities associated with a burner are primarily due to convective transport of fuel and oxidizer, and to some extent, due to the effects of burner wall. At lower fuel flow rates, the flame extinction is due to heat losses being higher than the heat release. At higher air and/or fuel flow rates, the flame extinguishes due to insufficient residence time, as well as due to the attainment of the lean limit. Additionally, when biogas is used, depending upon its carbon-dioxide content, the losses due to radiation add on to the instabilities.

In order to increase the operating range of the burner, flame stabilizers are often used. Flames stabilized in the presence of obstacles have been investigated theoretically, experimentally and numerically by many researchers. Experimental study of flame stabilization in the presence of an obstacle is carried out [18] and flow visualization was done using tracer particles (fine sodium salts). The images showed flame oscillations due to vortex shedding behind the bluff-body, as well as the occurrence of blow-off. Similar studies have been reported [19–23]. From these experiments, mixing patterns of burned and unburned gases were found to be distinct for streamlined and un-streamlined bodies [19], and the process of pre-heating of reactants by mixing with products in the recirculation zone [20] was shown. It was concluded that the recirculation zone present downstream the bluff-body was controlled by the flow dynamics rather than the reaction zone [21–23]. Many theoretical investigations were reported in the context of bluff-body flame stabilization [24–26] concluded that Damköhler number was an important parameter in understanding the flame stabilization. The effects of obstacles (backward facing step and bluff-body) on stability of cross-flow methane-air flames were experimentally studied [27] and reported stability maps for various configurations. They observed that the stability regime was dependent on the type and dimensions of the obstacles. The effects of obstacles on the structure of a cross-flow methane-air flames were numerically studied by [28–30]. The dependence of flame stability on step location and step height was shown and the predominance of step location was discussed. Through numerical simulations [29], the formation

of flame zone at locations, where the cell Damköhler number was nearly unity, was demonstrated. Experimental investigation of cross-flow methane-air flames in the presence of cylindrical bluff bodies of various shapes were also reported [31]. Stability maps for biogas-air cross-flow flames, without and with obstacles (backward facing step and bluff body) were presented [32]. Height and location of backward facing steps were varied. Detailed stability maps were presented in these works.

When considerable amount of carbon-dioxide, which is a diluent and thermal absorbing species, is present, the characteristics of biogas flames in cross-flow air can be quite different from the corresponding methane-air flames. Cross-flow flames allow higher operational control, especially when proper obstacles are used as flame stabilizers. Biogas being a promising alternative fuel, the characteristics of flames from biogas should be thoroughly understood. Detailed stability maps for biogas-air flames in different cross flow configurations without and with obstacles were reported [32]. Flame photographs were used to reveal different regimes of flames formed behind the obstacles. However, flow, temperature, species and reaction fields have not been measured because of probing difficulties. Such a data will be quite useful to understand the flame anchoring phenomena, resultant flow field and flame structure, which in turn helps in the design and optimize a burner. These data will be obtained using numerical study complementing the experimental study, will be quite useful, but is not available in literature. This forms the primary motivation of this study. Simulations of important experimental cases of biogas flames in cross-flow air, as reported in experiments [32], have been carried out. This study brings out a detailed analysis to understand the flow features, temperature and species fields near the flame stabilizers under different configurations. The present numerical simulations are able to show the basic differences in the flow fields behind backward facing step considering three cases: (a) isothermal cold flow of a single fluid (b) isothermal non-reacting flow of two fluids (fuel and air) and (c) the reacting flow. Further, the flame stabilizing mechanisms behind the backward facing steps of different sizes kept at different distances from fuel injection port are also revealed.

2. Numerical methodology

2.1. Computational domain

Fig. 1 shows the computational domain to simulate the experimental setup in Ref. [32] for cross-flow flames. From the experiments, the flames behind the backward facing steps are observed (from top view) to be two-dimensional in nature. ANSYS workbench 16.0 is used to create the two-dimensional domain and the mesh. The computational domain extends to 300 mm and 152 mm in x - and y -directions, respectively. A solid stainless-steel metal block of 150 mm \times 32 mm (length and depth) is present at the bottom, on the upstream side of the fuel injector

plate. Biogas (55% methane and 45% carbon-dioxide, by volume) is injected at required uniform velocity over a length of 70 mm. To the right of the fuel injector, another solid stainless-steel block of 80 mm \times 32 mm (length and depth) is present with its top surface in flush with the surface of the fuel injector. A stainless-steel wall of 300 mm length is present as the top surface at a distance of 120 mm from the bottom. Air enters uniformly from its inlet located at the left boundary and combustion products leave the domain through the right (pressure outlet). The backward facing step is also made of stainless-steel. The height (H) and distance (D) of the rear face of the backward facing step from the leading point of fuel injector are varied in the range of 5 mm to 15 mm, and 10 mm to 40 mm, respectively.

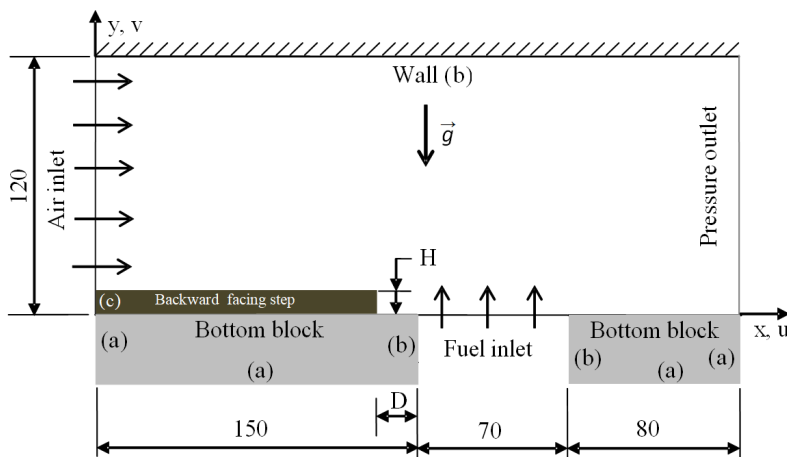


Fig. 1. Computational domain showing the boundary conditions in the presence of backward facing step (all units are in mm)

2.2. Boundary conditions

Air inlet: At this boundary, air is supplied at the required uniform velocity in the x -direction at a temperature of 300 K and at atmospheric pressure. The mole fraction of oxygen is 0.21 and that of nitrogen is 0.79.

Fuel inlet: The required uniform velocity of biogas is specified at the fuel inlet boundary. Mole fractions of methane and carbon dioxide are prescribed as 0.55 and 0.45, respectively. The fuel enters the domain at a constant temperature of 300 K. In experiments [32], the fuel is supplied through a porous ceramic plate to get a uniform velocity at the fuel surface. In this study, the porous plate has not been modeled due to the inherent complications involved. Therefore, it should be noted with a caution that there may be diffusion of products to the surface of the porous material. This can result in slight changes in the mole fractions of fuel mixture at the fuel inlet. Considering continuous supply of fuel mixture through

a pressure difference across the porous plate, the above assumption has been made. Also, considering the inert and adiabatic nature of the porous plate, the walls of the solid blocks adjacent to the fuel injector are considered adiabatic. It should also be noted with a caution that this is a simplified condition considering the non-trivial nature of conjugate heat transfer occurring in experiments at the interface of porous material and the solid metal blocks on either side. These two simplifying assumptions are incorporated considering the scope of this work, where only a relative comparison is being made between several cases simulated to bring out the flame characteristics.

Wall: All the walls, no slip condition ($u = v = 0$) is specified for velocity. The first derivatives of mass fractions of all species normal to the wall are set to zero. Top wall is considered as adiabatic. In bottom solid blocks, the wall boundaries indicated as “a” are treated as convective heat transfer surfaces, and are prescribed with a natural convective heat transfer coefficient of $10 \text{ W/m}^2\text{K}$ and ambient temperature of 300 K. The wall surfaces indicated as “b” are considered as adiabatic, as mentioned earlier. One of the walls of the backward facing step, indicated by “c”, is considered to be isothermal at 300 K. A coupled boundary condition is specified for all the remaining wall surfaces, which are in contact with the fluid zone within the computational domain. Here, heat interaction between the fluid and solid takes place.

Pressure outlet: The combustion products leave to the atmosphere through this boundary. Atmospheric pressure of 1 bar is prescribed at the outlet. In the case of a negative pressure gradient (favorable), all variables (other than pressure) at this boundary are calculated by extrapolation from the adjacent interior cells; the first spatial gradient of all the flow variables is set to zero at this boundary. However, if the local pressure gradient is positive (adverse pressure gradient) at this boundary, air (21% oxygen and 79% nitrogen by volume) will enter the domain with a temperature of 300 K.

2.3. Models and discretization schemes

Governing equations for conservation of mass, species, momentum and energy are solved in a segregated manner using ANSYS FLUENT 16.0. If the flame is observed to be unsteady, as observed by fluctuations in the values of the residuals, then time dependent equations are solved using a time step of 10^{-5} s, keeping the steady state solution as the initial condition. SIMPLE (Semi-Implicit Method for Pressure Linked Equations) algorithm is used to handle pressure velocity coupling. Gradient-based least square cell method is used for spatial discretization of pressure. Second order upwind scheme is employed for spatial discretization of convective quantities. Diffusion energy source is used to include the transport of enthalpy by the diffusing species in the energy equation. The overall chemical kinetics mechanism for methane combustion, consisting of C_1 and C_2 carbon species,

is used. Laminar finite rate model, which uses Arrhenius type rate equations, is employed to find the net reaction rate of a species, using a stiff chemistry solver.

2.4. Chemical kinetics mechanism

A short chemical kinetics mechanism, which has 25 species and 121 elementary reactions, is used for modeling combustion. This chemical kinetics mechanism is obtained from GRI 2.11 mechanism after removing the hydrocarbons higher than C_2 and the species containing nitrogen atom, except N_2 . The species present in the mechanism are: H_2 , H , O , O_2 , OH , H_2O , HO_2 , H_2O_2 , CH , CH_2 , CH_3 , CH_4 , CO , CO_2 , HCO , CH_2O , CH_3O , C_2H , C_2H_2 , C_2H_3 , C_2H_4 , C_2H_5 , C_2H_6 , $HCCO$ and N_2 . The kinetics used by [28] has 18 species, without C_2 species. Since, biogas has a significant amount of CO_2 , higher amounts of CO will be formed through elementary reactions such as $O + CO_2 \leftrightarrow CO + O_2$ and $H + CO_2 \leftrightarrow OH + CO$. The resultant higher concentration of CO enables the formation of C_2 species, as well as react with them to produce radicals. A few elementary reactions illustrating these are: $CO + CH \leftrightarrow C_2H + O$, $CO + CH_3 \leftrightarrow OH + C_2H_2$ and $CO + C_2H_2 \leftrightarrow CH + HCCO$. It is well known that both C_1 and C_2 mechanisms, which incorporate elementary reactions of GRI 2.11, predict the methane oxidation quite precisely and C_2 species take care of additional effects of CO_2 present in reactant mixture.

2.5. Radiation sub-model

Soot emissions are not significant in biogas flames in cross-flow air under atmospheric conditions. However, thermal radiation absorption by absorbing species such as CO_2 , CO , H_2O and CH_4 is important and has to be considered to predict the temperature in a realistic manner. Therefore, a volumetric radiation sub-model [33], which is based on optically thin approximation, is employed. Using the Planck's absorption coefficients for the absorbing species, calculated as a function of temperature and species mole fractions, the thermal energy loss due to radiation is calculated [33]. This radiation heat loss term is implemented in ANSYS Fluent as a volumetric negative source term in the energy equation using a User Defined Function (UDF), written in C language.

2.6. Solution procedure

A case with a stable flame, with a low air flow rate is chosen first. All the boundary conditions are specified appropriate for the case. Steady state governing equations are solved without including the volumetric reactions for around 2000 iterations. At this stage, the flow is sufficiently established and flammable mixture is formed. A temperature of 1800 K is initialized at a selected small area near the leading edge of the fuel inlet to onset ignition. The reactive flow is solved in a steady state manner. If the case has steady solution, the residuals gradually decrease to

the required criteria. The normalized residual value has to be less than 1×10^{-3} for continuity, less than 10^{-4} for momentum and species, and below 1×10^{-6} for energy. At least 60000 iterations are executed before the convergence is checked. A computational time of around 70 hours is required to execute 60000 steady state iterations in an Intel (R) Core (TM) i7-4790 at 3.6 GHz processor workstation, employing 6 cores. The mass imbalance, calculated as the ratio of net mass efflux to the minimum incoming mass, is ensured to be less than 1% for all cases. The steady state convergence is also checked by plotting the profiles of variables such as temperature, velocity and species mass fractions at several x -locations. If the case is observed to be unsteady, as indicated by the fluctuating residual values, unsteady governing equations are solved with a time step of 1×10^{-5} s. The solution is converged with sufficient number of iterations within a time step. Based on the flow time, calculated as the length of the fuel injector divided by the air velocity, the total time period of the transient simulation is calculated and time averaging of the data is carried out. For a transient simulation with a timestep size of 10^{-5} s, approximately 90 hours are needed to run for a time duration of 1 s in an Intel (R) Core (TM) i7-4790 at 3.6 GHz processor workstation, employing 6 cores. Starting from the case of the stable flame, gradual modifications to air and fuel velocities are done to simulate the flames in various regimes. Steady state solution for steady cases and time averaged solution for transient cases have been employed for analysis.

2.7. Validation

After carrying out a grid independence study, a structured grid with 93220 non-uniform quadrilateral cells is used in the present simulations. The minimum cell size is 0.5 mm, placed near the walls and the flame zones. The solid blocks and the backward facing step are also meshed and conjugate heat transfer is solved. Numerical results for methane flame in cross-flow air have been validated using the experimental data from literature [34]. Further, experimental results for biogas flames in terms of temperature and velocity measurements are not available in literature. It is difficult to make probed measurements of temperature in biogas flames [32]. Therefore, a qualitative validation of the numerical results for biogas flames has been carried out in this study as shown in Figs. 2 and 3.

Using the high-definition flame photographs of biogas-air flames [32], the visible flame extents have been compared with predicted contours of OH in Fig. 2. Here, fuel velocity of 0.021 m/s and air velocity of 0.4 m/s are used in different configurations with backward facing steps. The step height (H) and location (D) have been varied in the range of 5 mm to 10 mm, and 10 mm to 40 mm, respectively. This set of fuel and air velocities produces flames anchored in the plate region between the leading point of fuel injector and the rear surface of the backward facing step. It is clear from Fig. 2 that the predicted OH contours are able to delineate the visible flame extents including the anchoring locations quite clearly

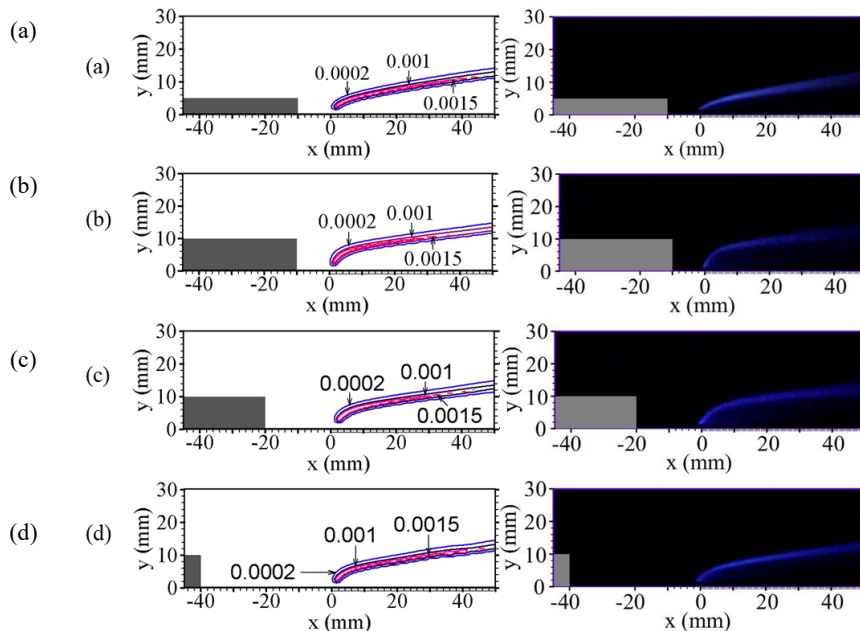


Fig. 2. Comparison of predicted OH contours and experimental flame images for fuel velocity of 0.021 m/s and air velocity of 0.4 m/s, for: (a) $H = 5$ mm, $D = 10$ mm, (b) $H = 10$ mm, $D = 10$ mm, (c) $H = 10$ mm, $D = 20$ mm and (d) $H = 10$ mm, $D = 40$ mm

observing OH contour line of 0.001. The reactive layer thicknesses are also captured quite well.

To verify the capability of the numerical model to predict a different regime of flame that is not anchored to the plate region, the cases with the fuel velocity of 0.021 m/s and a higher air velocity of 1.7 m/s have been considered. Fig. 3 presents the predicted OH contours in comparison to direct flame photographs for the cases with three step heights (5 mm, 10 mm, and 15 mm) and three step locations (10 mm, 20 mm, and 40 mm). It is observed that these flames are flat and lifted from the plate region. Such flames are partially premixed flames, where some amount of air mixes with biogas before reaching the combustion zone. It should be noted that the case with step height of 10 mm and step location of 40 mm is oscillatory and time averaged OH contours are shown to indicate the reaction zone thickness. It is clear from Fig. 3 that the numerical model is also able to predict the flames quite satisfactorily for this set of air and fuel velocity. Numerical predictions compare well with the experimental flame extents, including the anchoring regions. This validation exercise suggests that the numerical model can be used to assess the relative differences in the flow, thermal, species and reaction fields between various configurations and to avail detailed physical insight of the flow field and flame structure.

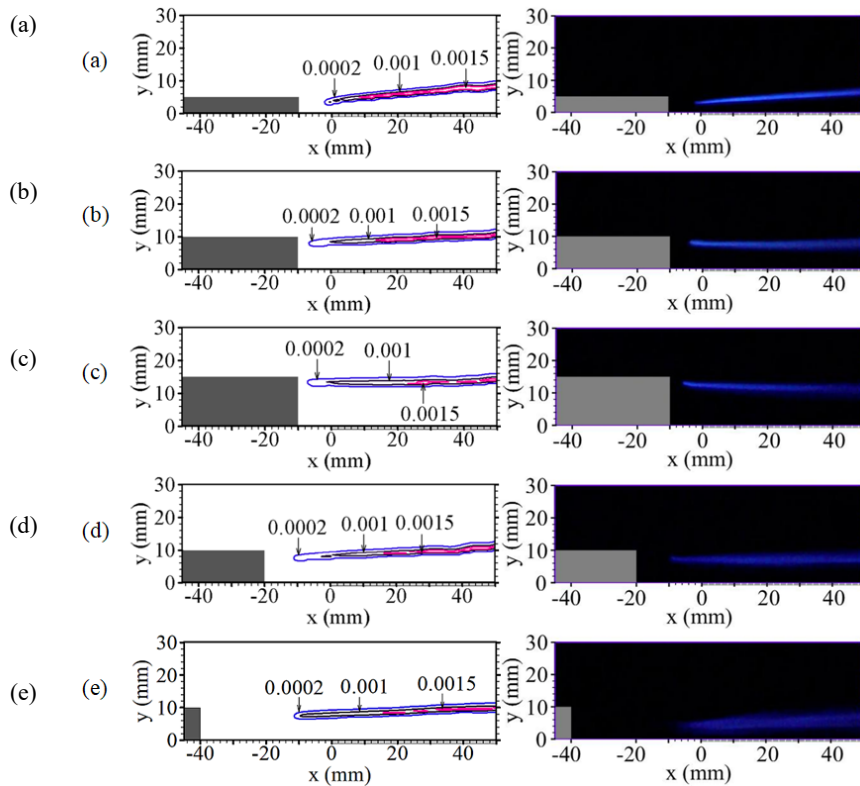


Fig. 3. Comparison of predicted OH contours and experimental flame images for fuel velocity of 0.021 m/s and air velocity of 1.7 m/s, for: (a) $H = 5$ mm, $D = 10$ mm, (b) $H = 10$ mm, $D = 10$ mm, (c) $H = 15$ mm, $D = 10$ mm and (d) $H = 10$ mm, $D = 20$ mm, (e) $H = 10$ mm, $D = 40$ mm

3. Results and discussion

The flame configurations formed behind a backward facing step are categorized as plate stabilized, lifted, step stabilized and separated flames [32]. These regimes depend upon parameters such as fuel and air velocity, step height, and step location. In the parametric study, step heights (H) of 5 mm, 10 mm and 15 mm, located at a distance (D) of 10 mm from leading point of fuel injector, are simulated. For a given fuel velocity, when air velocity is gradually increased, four flame regimes are formed [32]. Therefore, fuel velocities of 0.021 m/s and 0.046 m/s are considered. Similarly, the simulations show that the length of the fuel injector does not play a significant role for a given set of fuel and air velocities. Thus, fuel injector length is kept as 70 mm. The effect of step location is studied for $H = 10$ mm, by varying D as 10 mm, 20 mm and 40 mm. The characteristics of these flames have been reported in detail.

3.1. Reactive and non-reactive flow fields

Flow field behind the step is quite different for cases with and without reactions. To understand the distinct features of flow fields, three cases are considered behind a step of $H = 10$ mm located at $D = 10$ mm. In the first case (case 1), only air is fed in x -direction at a given velocity. No fuel is injected and the fuel injector is considered as a no-slip wall. Isothermal simulation at 300 K has been carried out. The second case (case 2) considers fuel injection in addition. However, no reaction is considered. Fuel and air mix at isothermal conditions in this case. The fuel air mixture formed in case 2 is ignited and a reactive flow is established in case 3.

Fig. 4 shows the flow field in terms of streamlines and velocity vectors (to show the magnitude) behind the 10 mm step for the three cases. For case 1 (Fig. 4a), a large clock-wise recirculation vortex is seen behind the step. This vortex extends to approximately 90 mm from the rear face of the step. In the second case, two recirculation zones, one clockwise formed near the top portion of the step, and another anti-clockwise, formed towards the bottom of the step are observed as shown in Fig. 4b. Due to cross movement of fuel and air streams, a stagnation region forms around $x = 5$ mm and $y = 9$ mm, and this bifurcates the two oppositely rotating vortices. It is clear that to the right of this stagnation point, fuel stream accelerates and flows along with the air stream. The presence of the step has enabled thorough mixing of fuel and air behind it.

At these conditions, when the mixture is ignited, a plate stabilized flame is established (discussed later) and the counterclockwise vortex vanishes (Fig. 4c).

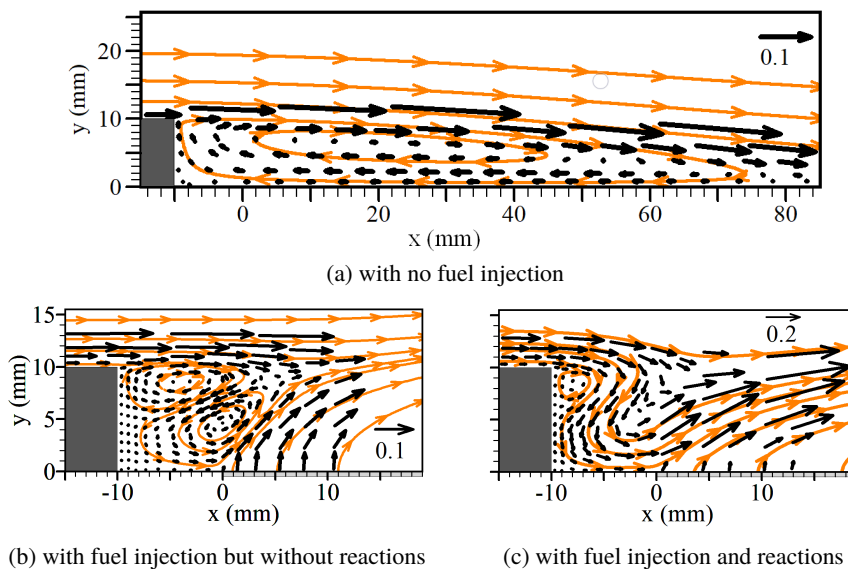


Fig. 4. Streamlines and velocity vectors behind the step for various cases. The fuel and air velocities are 0.046 m/s and 0.4 m/s, respectively

The clockwise recirculation zone near the top portion of the step becomes weaker. In a reactive flow, the hot gases accelerate across the flame zone, as indicated by higher magnitude velocity vectors in Fig. 4c. This pulls out the mixture in the wake region of the step into the flame zone, distorting the anti-clockwise vortex. Clearly, air stream fills up the wake region and flows horizontally over the plate region between the step and leading edge of the fuel inlet. Fuel is not able to penetrate much into the wake region.

Another case with a higher air velocity of 1.4 m/s and with the same fuel velocity has been executed. Without any fuel flow (the fuel injector treated as wall), a clockwise recirculation zone with a reattachment length greater than 90 mm is formed, as shown in Fig. 5a, due to the increased air momentum.

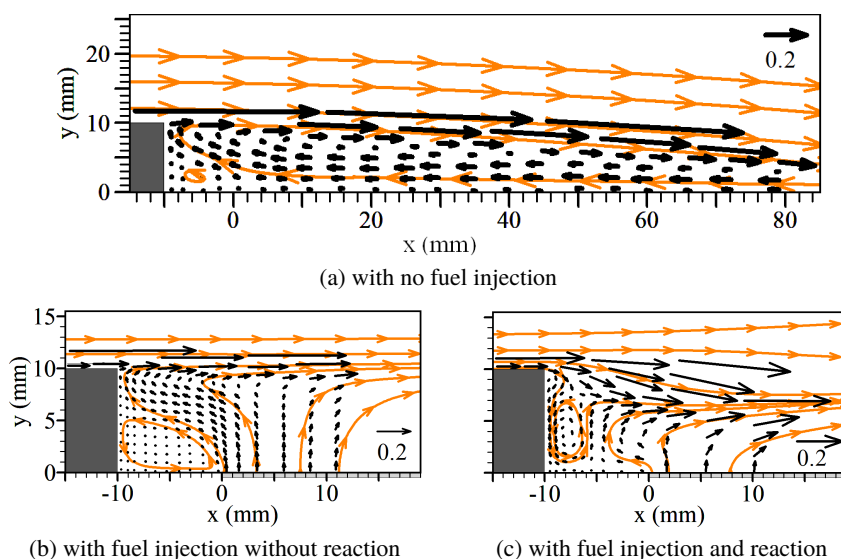


Fig. 5. Streamlines and velocity vectors behind the step for various cases. The fuel and air velocities are 0.046 m/s and 1.4 m/s, respectively

For the case with fuel supply, but no reactions, a much weaker anti-clockwise vortex is found near the bottom portion of the rear face of the step. Clearly, the air flow is restricted in the wake region near the top rear face of the step, enabling the fuel to be transported towards the step, as shown in Fig. 5b. When ignited, a step stabilized flame is formed in this case (discussed in more detail later). Due to the formation of the flame, a stream flowing downwards, almost parallel to the rear face of the step, is seen (Fig. 5c). Now, a bigger anti-clockwise vortex is observed in the wake. Fuel transported towards the step, gradually diffuses into this vortex, where it mixes with air. Apparent acceleration of flow across the flame zone is observed. The effects of fuel injection in non-reacting environment and those of chemical reactions behind the step on the resultant flow field are seen clearly from Figs. 4 and 5.

3.2. Effect of air velocity on flame anchoring

Keeping the fuel velocity at 0.046 m/s, the air velocity is varied in the range of 0.4 m/s to 1.4 m/s for the case with $H = 10$ mm, $D = 10$ mm. At 0.4 m/s, a plate stabilized flame forms, as shown in left side of Fig. 6a. However, due to heat losses through the plate, the flame anchors a few mm away from the plate surface. The flame resembles the shape of a laminar boundary layer. The isotherms along with stoichiometric contour line ($\phi = 1$), shown as a dashed line, are presented on the left side of Fig. 6a, reveals this trend. The stoichiometric contour line is calculated as, $Y_{\text{methane}} - Y_{\text{oxygen}}/\nu = 0$, where Y is mass fraction and ν is mass of oxygen required to burn one kg of methane ($\nu = 4$). Stoichiometric contour line is attached to the plate region just upstream of the leading point of the fuel injector and it is close to the high temperature zone of 1850 K.

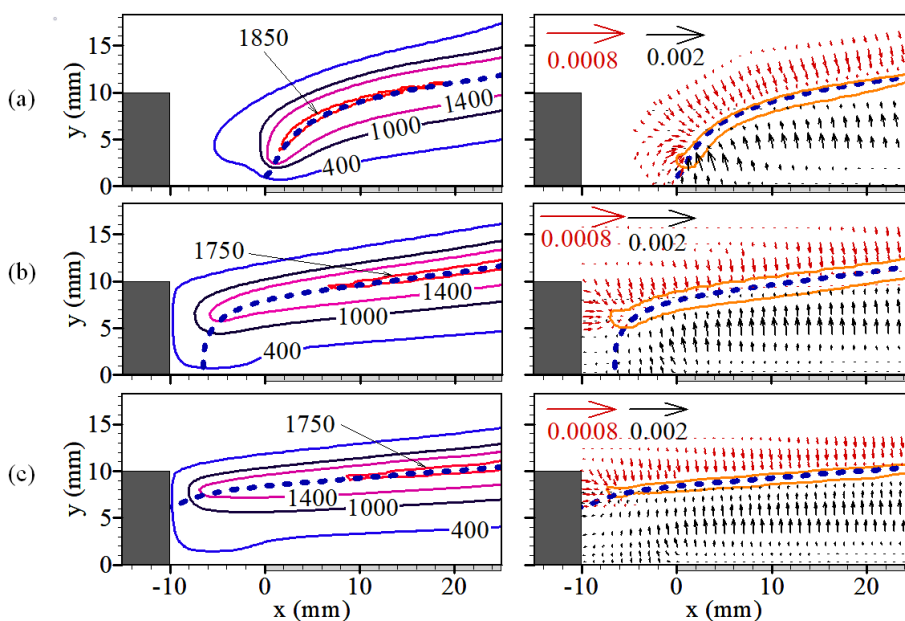


Fig. 6. Contours of temperature (in K, left side), Net Reaction Rate (NRR) of CH₄ (right), diffusion mass flux vectors of methane and oxygen along with contour line of $\phi = 1$ (dashed line) for fuel velocity of 0.046 m/s and air velocity of (a) 0.4 m/s, (b) 0.8 m/s and (c) 1.4 m/s for $D = 10$ mm, $H = 10$ mm

Diffusion of fuel and oxygen, represented by the diffusion flux vectors, towards the flame zone depicted by the net reaction rate (NRR) contours of methane with a value of -1 kg/(m³s), is shown on the right side of Fig. 6a. The diffusion mass flux of methane is higher at the leading point of fuel injector. A slight oxygen leakage into the fuel zone by diffusion through the small gap in the flame anchoring point is observed. Stoichiometric contour line lies within the contour line of NRR of

methane with a value of $-1 \text{ kg}/(\text{m}^3\text{s})$. As the air velocity is increased to 0.8 m/s , the flame lifts-off from the plate region and moves towards the rear face of the step, forming a lifted flame (Fig. 6b).

Clearly, the curvature of isotherms and that of $\phi = 1$ line have changed as shown in the left side of Fig. 6b. Even though, $\phi = 1$ line is attached to the plate region, high temperature zones have formed away from the plate surface. This is because diffusion flame forms in a region where Damköhler number (Da) is around 1.0 ([26] and [29]). Damköhler number (Da) is the ratio of flow residence time to the reaction time. In the present study, Da is calculated in each cell of the domain. Flow time is calculated as the cell size (length) to the average velocity in the cell in the x-direction. The reaction time is calculated as the ratio of net reaction rate of methane to the density of methane in the particular cell. NRR of methane on the right column of Fig. 6b depicts the anchoring of reaction zone and the lifted nature of the flame. Diffusion of oxygen into the reaction zone is higher near the leading edge of the flame (Fig. 6b, right). Close to the plate region between the rear face of the step and the fuel injector, some amount of methane and oxygen diffuse and partially pre-mix. Thus, the lifted flame is not entirely a non-premixed flame, but a partially premixed flame.

A step stabilized flame is formed at an air velocity of 1.4 m/s (Fig. 6c). It is evident that the flame has become nearly flat as observed from the isotherms (left) and NRR of methane represented by its contour line of $-1 \text{ kg}/(\text{m}^3\text{s})$ (right) as shown in Fig. 6c. The contour line of $\phi = 1$ now anchors to the trailing edge of the step. The mode of combustion is predominantly non-premixed at this regime, with a small leakage of oxygen through the small gap between the flame anchoring point and rear face of the step, as shown in right column of Fig. 6c.

The oxygen transport and the flow field behind the backward facing step are analyzed for these cases. For the plate stabilized flame, oxygen penetrates up to the plate region, as shown in Fig. 7a. Air flow bends towards the rear step surface and mixes with the fuel stream. Flow acceleration across the flame zone is clearly seen. The distinct nature of this flow field has been compared with non-reacting flow fields in Fig. 4a. The blowing fuel velocity and the reaction zone that accelerates the gases across it, form the reason for the distinct flow field formed behind the step. Since the flame sustains a few mm away from the plate surface, oxygen diffusion across the flame zone is evident as shown by the contour line with oxygen mass fraction of 0.02. The fuel transport is not by convection for this case as seen from the vectors.

As the flame lifts-off at higher air velocity of 0.8 m/s , the oxygen penetration is clearly restricted, as shown in Fig. 7b. Air flows parallel to the rear surface of the step and flows towards the fuel stream. The acceleration across the flame zone is apparent. By observing the isotherms in Fig. 6b and the flow field in Fig. 7b, it is clear that the anchoring point of the flame is in the low velocity zone, around the center of the vortex field in the wake region. Increased fuel blowing effect is seen as the horizontal component of velocity in the wake region is smaller for this case

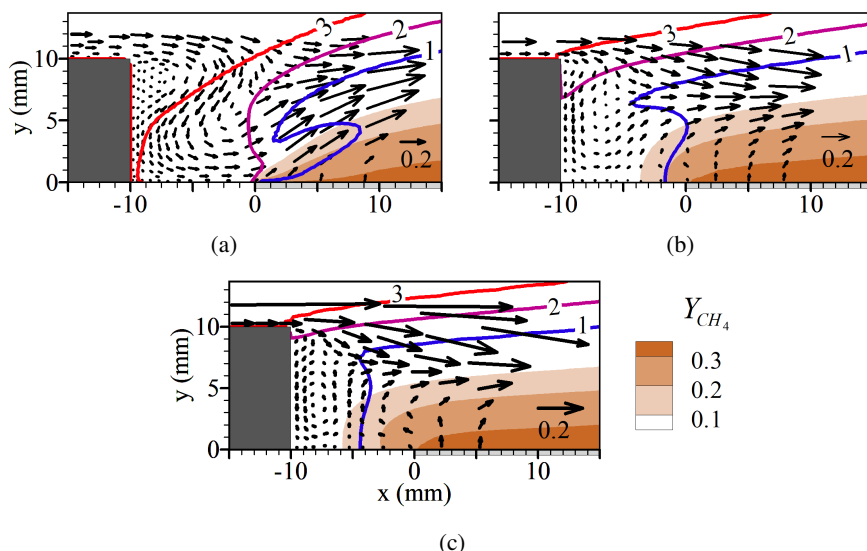


Fig. 7. Contours of mass fraction of oxygen (lines), methane (greyscale) along with mixture velocity vectors at fuel velocity of 0.046 m/s and air velocities of (a) 0.4 m/s, (b) 0.8 m/s and (c) 1.4 m/s, behind a step of $D = 10$ mm, $H = 10$ mm. [O_2 labels: 1: 0.02, 2: 0.16, 3: 0.23]

as compared to the plate stabilized case. Convective movement of fuel towards the oxygen is seen only near the leading edge of the fuel injector.

At further higher air velocity of 1.4 m/s, oxygen penetration in the rear region of the step has further decreased (Fig. 7c). The flow field near the rear step surface is similar to that of the lifted flame; however, with a much smaller anti-clockwise recirculation. Clear convective transport of fuel towards the flame zone is observed from the velocity vectors. Fuel transport deeper into the wake region of the step enables the formation of a step-stabilized flame for this case. Flame acceleration across the flame is evident as in the previous cases.

Species distributions are studied with the help of CO and H_2O mass fraction contours in Fig. 8. Here, the contour line of OH with a value of 0.001 has been included (dashed line) to show how OH consumption aids the formation of CO_2 through CO, and H_2O . The distributions of CO and H_2O are restricted to the zone above the fuel injector plate for the plate stabilized flame as shown in left and right sides of Fig. 8a, respectively. For the lifted and step stabilized flames, CO and H_2O are distributed upstream of the fuel injector also, as shown in Figs. 8b and 8c, respectively. However, the maximum zones of CO and H_2O are seen in the upper portion of the fuel injector surface. The maximum value of CO decreases, as the air velocity is increased and its location moves downstream. The maximum value of H_2O has not changed much and its location is seen to move downstream with an increase in the air velocity. The consumption of CO and formation of H_2O are clearly aided by OH. The contour line of OH with a value of 0.001 is seen in the

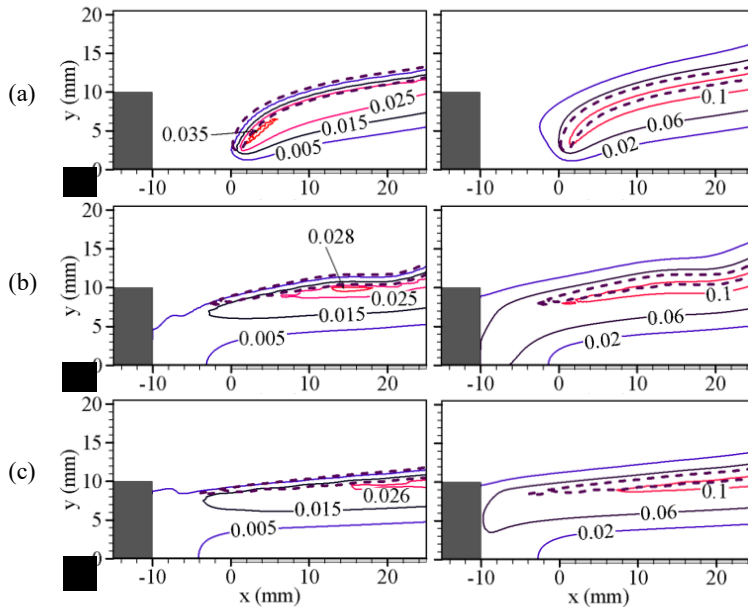


Fig. 8. Contours of mass fractions of CO (left) and H₂O (right) along with mass fraction contour line of OH = 0.001 (dashed line) at fuel velocity of 0.046 m/s and air velocities of (a) 0.4 m/s, (b) 0.8 m/s and (c) 1.4 m/s, behind a step of $D = 10$ mm, $H = 10$ mm

upper layer of CO, where it is consumed to form CO₂. On the other hand, it is seen to be interlinked with maximum value of H₂O indicating its formation in a layer below.

3.3. Effect of step height on flame dynamics

The effect of step height on reactive flow field is reported in this section. The step height (H) has been varied from 5 mm to 15 mm and the location (D) is kept as 10 mm. For $H = 15$ mm, the flame is highly oscillatory. For this case, transient simulations are carried out and time averaged variables are used in the contours. Fuel is injected at a velocity of 0.021 m/s. At a low air velocity of 0.4 m/s, plate stabilized flame is formed for the three cases. Fig. 9 shows the isotherms along with contour line of $\phi = 1$ in its left column and contours of mass fractions of O₂ and CH₄, along with velocity vectors, in its right column. Contour line of $\phi = 1$ anchors close to the leading edge of the fuel injector for all step heights. Isotherm with a value of 1400 K anchors close to the leading edge of the fuel injector, a few mm away from the plate surface (Fig. 9a). The flame curvature increases with an increase in the step height due to the differences in the penetration of fuel and oxygen in the wake region as the step height is varied. Mass fraction contours of oxygen along with mixture velocity vectors for plate stabilized flames are shown on the right column of Fig. 9. For this combination of air and fuel velocities, at the

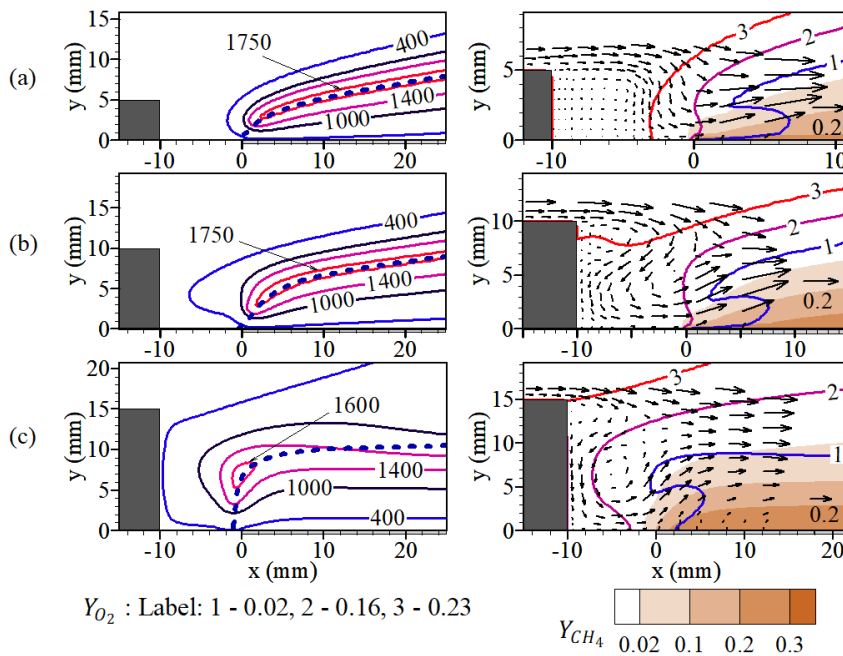


Fig. 9. Contours of temperature along with contour line of $\phi = 1$ (dashed line) (left) and mass fractions of methane (greyscale), oxygen (lines) and velocity vectors at fuel and air velocities of 0.021 m/s and 0.4 m/s, respectively, for $D = 10$ mm, and: (a) $H = 5$ mm, (b) $H = 10$ mm, (c) $H = 15$ mm

step height of 5 mm (Fig. 9a, right), oxygen penetrates well behind the step and the oxygen mass fraction contour line of 0.21 is seen close to the leading edge of the fuel injector.

Here, a weak clockwise recirculation zone is observed behind the step. For 10 mm step height, the clockwise recirculation zone behind the step has decreased in size and has moved towards the top of the step (Fig. 9b, right). The flow bends towards the step and directs itself horizontally towards the fuel stream at the bottom. Oxygen penetration, following contour lines labeled 1 and 2, is almost similar to that observed for 5 mm step height. For the step height of 15 mm (Fig. 9c, right), a counterclockwise flow field is observed at the bottom of the rear surface of the step. Oxygen contour line of 0.21 is seen to be attached to the step; however, it is clear that oxygen has penetrated to the region behind the step. In all these cases, flow acceleration is observed across the flame zone.

When the velocity of air is increased to 0.8 m/s, the flame is just lifted for $H = 5$ mm, clear lifted flame is obtained for $H = 10$ mm, and the lifted flame transitioning to a step stabilized flame is obtained for $H = 15$ mm, as observed from the isotherms in the left column of Fig. 10. For the case of $H = 15$ mm, the flame is oscillatory with a steady solver and a transient solver has been used. Time averaged values are reported for this case. The maximum temperature decreases,

as H is increased from 5 mm to 10 mm. Its location moves downstream when H is further increased to 15 mm. Stoichiometric contour line attaches to the step for $H = 15$ mm.

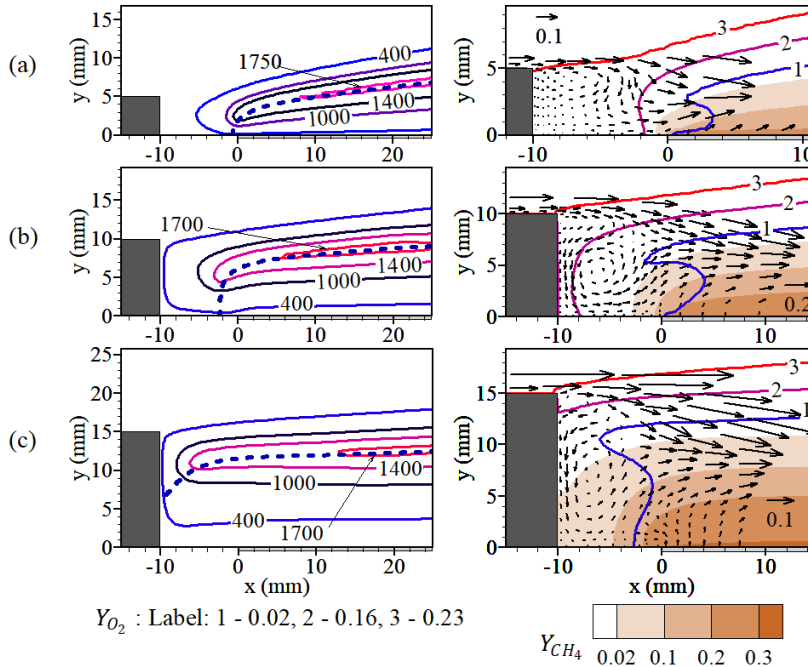


Fig. 10. Contours of temperature along with contour line of $\phi = 1$ (dashed line) (left) and mass fractions of methane (greyscale), oxygen (lines) and velocity vectors at fuel and air velocities of 0.021 m/s and 0.8 m/s, respectively, for $D = 10$ mm, and: (a) $H = 5$ mm, (b) $H = 10$ mm, (c) $H = 15$ mm

Oxygen penetration behind the rear surface of the step is clearly seen for $H = 5$ mm (Fig. 10a, right). A clockwise vortex near the top of the step transports oxygen towards the leading edge of the fuel injector as indicated by the velocity vectors. This vortex has become smaller and stronger than the one observed in the case of the plate stabilized flame (Fig. 9a, right). For the case of $H = 10$ mm, a small clockwise at the top and an anti-clockwise vortex near the bottom appears behind the step as shown in Fig. 10b, (right). This flow structure is similar to that of step stabilized flame for $H = 15$ mm at the lower air velocity of 0.4 m/s (Fig. 9c, right). Due to the combined effects of increased flow inertia and fuel convection into the wake region, oxygen penetration behind the step has been restricted by this flow field, as indicated by the contour lines of oxygen mass fraction.

For the step height of 15 mm, a counterclockwise vortex is observed behind the step and oxygen penetration is further restricted by this flow field as shown in Fig. 10c, (right) by the contour line of 0.16. This is due to the increased length scale of the wake as well as fuel injection. The fuel has to travel a longer distance

vertically to mix with required amount of oxygen, forming the flame zone away from the plate region. A smaller and weaker clockwise vortex is also observed near the top of the step (Fig. 10c). For a given fuel and air velocity, it can be concluded that the flame lift-off occurs for higher step height at a lower air velocity as observed in experiments [32].

For the fuel velocity of 0.021 m/s, when the velocity of air is increased to 2 m/s, clear step stabilized flames are formed for $H = 10$ mm and 15 mm, and a flame transitioning from lifted to step stabilized regime is observed for $H = 5$ mm (Fig. 11). For $H = 5$ mm, the flame has become flatter, however, not completely attached to the step (Fig. 11a, left). In fact, for this smaller step height, as per the experimental observations [32], step stabilized flames are flat, but they anchor little away from the rear face of the step. The reason for this is due to the clockwise vortices formed in the case of 5 mm step, which transport air towards the leading point of fuel injector (Fig. 11a, right). This vortex is weaker to carry the fuel close to the rear face of the step. The anti-clockwise vortices in $H = 10$ mm and 15 mm, are able to transport the fuel towards the rear face, when oxygen is unable to penetrate in the wake region (Figs. 11b and 11c, right).

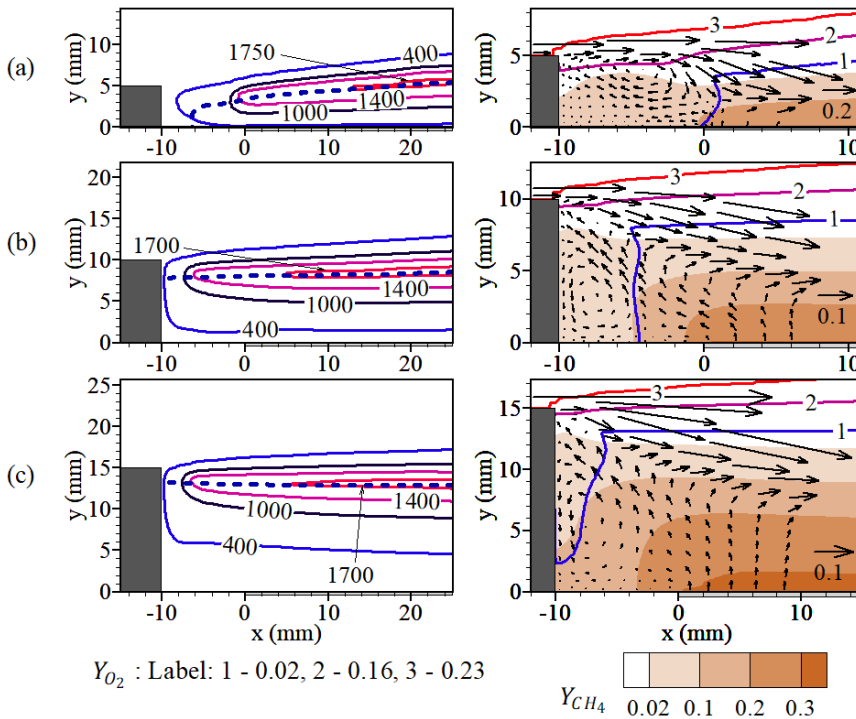


Fig. 11. Contours of temperature along with contour line of $\phi = 1$ (dashed line) (left) and mass fractions of methane (greyscale), oxygen (lines) and velocity vectors at fuel and air velocities of 0.021 m/s and 2 m/s, respectively, for $D = 10$ mm, and: (a) $H = 5$ mm, (b) $H = 10$ mm, (c) $H = 15$ mm

For $H = 10$ mm and 15 mm, the flames anchor near the top corner of the step, with almost the same maximum temperature values and locations. The isotherm of 1400 K reveals that the flames in 5 mm, 10 mm and 15 mm steps are positioned around -1 mm, -6 mm and -7 mm, respectively, from the leading point of the biogas injector (Fig. 11, left). As the step height is increased, the oxygen penetration into the wake region decreases, as indicated by the oxygen mass fraction line of 0.02 (Fig. 11, right).

3.4. Effect of step location on flame dynamics

The effect of the step location (D) on the characteristics of flames in various configurations are reported in this section. The step height (H) is kept as 10 mm and the location of its rear surface from the leading edge of the fuel injector (D) has been varied as 10 mm, 20 mm and 40 mm. The fuel velocity is kept as 0.021 m/s. At a low air velocity of 0.4 m/s, a plate stabilized flame is formed for the three cases of varying D . Fig. 12 (left) presents the isotherms and stoichiometric contour lines and Fig. 12 (right) presents the contours of mass fractions of methane, oxygen and mixture velocity vectors.

The maximum temperature and its location with respect to the fuel injector have not changed as D is varied (Fig. 12, left). The flame anchoring and its extents

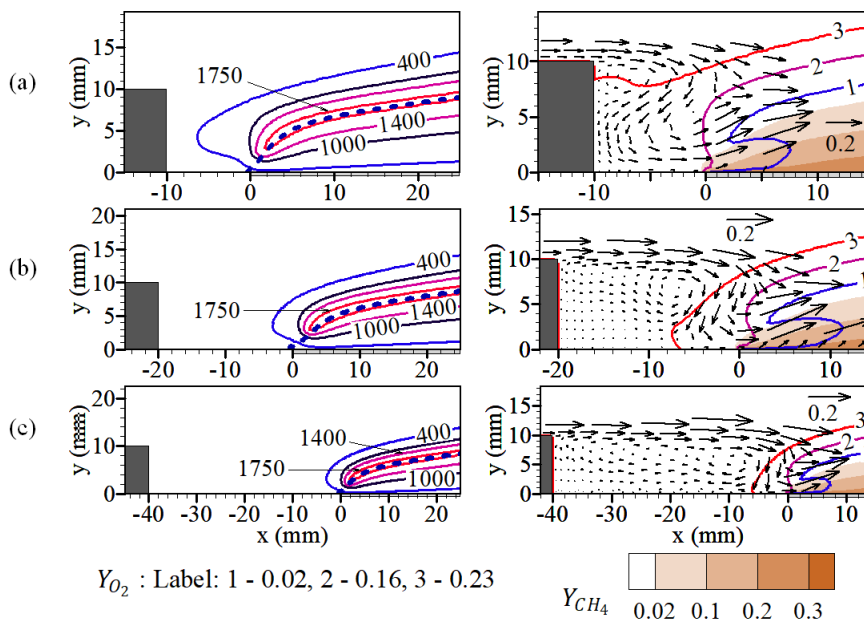


Fig. 12. Contours of temperature along with contour line of $\phi = 1$ (dashed line) (left) and mass fractions of methane (greyscale), oxygen (lines) and velocity vectors at fuel and air velocities of 0.021 m/s and 0.4 m/s, respectively, for $H = 10$ mm, and: (a) $D = 10$ mm, (b) $D = 20$ mm, (c) $D = 40$ mm

are also almost the same for the three cases, as indicated by the stoichiometric contour line. It is interesting to note the formation of a clockwise vortex in the wake region, and its movement away from the rear face of the step as the step location is increased. The dependence of the flow field on the fuel supply is noted by the inverted S type streamlines forming just upstream of the fuel injector (Fig. 12, right). The pattern of this flow field is also almost similar for the three cases. The clockwise vortex extends in the flow direction to accommodate the formation of this pattern. Other usual features, such as acceleration of hot gases across the flame zone and non-penetration of fuel into the wake region, are observed as in previous discussions with respect to plate stabilized flames. At a higher air velocity of 0.8 m/s, almost lifted flames are formed for all step locations, as shown in Fig. 13. This is indicated by the perpendicular anchoring of the stoichiometric contour lines and by the movement of the maximum temperature zone (Fig. 13, left). The maximum temperature slightly increases, as D is increased to 40 mm, indicating the onset of partial premixing. Like in the previous cases with plate stabilized flames, it is quite interesting to note that only small differences are observed in the overall flame structure, even when the wake flow field has quite a lot of distinct features when D is varied in the range of 10 mm to 40 mm.

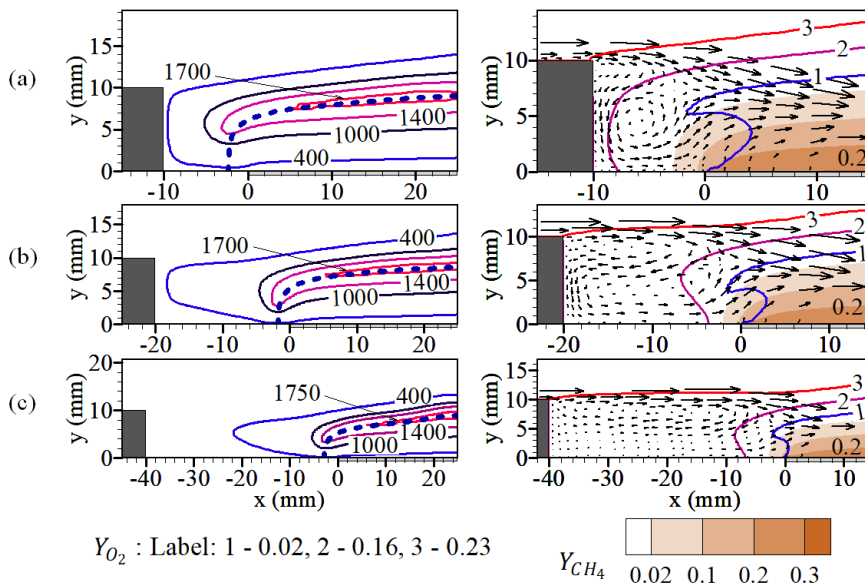


Fig. 13. Contours of temperature along with contour line of $\phi = 1$ (dashed line) (left) and mass fractions of methane (greyscale), oxygen (lines) and velocity vectors at fuel and air velocities of 0.021 m/s and 0.8 m/s, respectively, for $H = 10$ mm, and: (a) $D = 10$ mm, (b) $D = 20$ mm, (c) $D = 40$ mm

A strong counter-clockwise recirculation is observed behind the step located at 10 mm, as shown on the right side of Fig. 13a, (right). When the step location is increased to 20 mm, a vortex pair of clockwise rotation on the top and counter-

clockwise rotation at the bottom is observed behind the step as shown in Fig. 13b, (right). For the step location of 40 mm, a longer clockwise rotating vortex is observed behind the step (Fig. 13c, right) located above the plate. In all these cases, the oxygen penetration looks similar following the contour lines of oxygen mass fraction with values of 0.02 and 0.16. The fuel penetration upstream of the injector is also quite similar in all the three cases.

For the fuel velocity of 0.021 m/s, when the air velocity is further increased to 1.6 m/s, a clear step stabilized flame is formed in the case of $D = 10$ mm, as shown by the isotherms and stoichiometric contour line in Fig. 14a, (left). Here, the flame is flat and anchors close to the step. When the step location is increased to 20 mm and further to 40 mm, even though the flames become flatter, the stoichiometric contour lines anchor to the plate region (Figs. 14b and 14c, left). Following the 1400 K isotherm, it is clear that the primary reaction zone extends only up to a certain distance (around 7 mm to 12 mm) upstream of the fuel injector for all the three cases.

The maximum temperature and its location are also much similar between the three cases. The case of step location of 40 mm is transient in nature and time averaged variables are used in contour plots. As D increases, the flame anchors at a larger distance from the step. Counterclockwise recirculation zones are observed for all cases just behind the rear surface of the step (Fig. 14, right). However, for

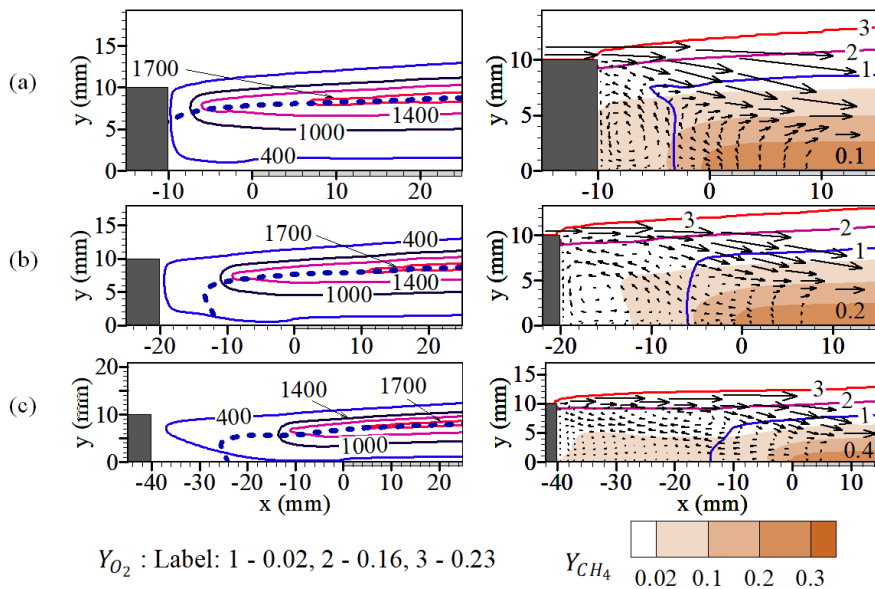


Fig. 14. Contours of temperature along with contour line of $\phi = 1$ (dashed line) (left) and mass fractions of methane (greyscale), oxygen (lines) and velocity vectors at fuel and air velocities of 0.021 m/s and 1.6 m/s, respectively, for $H = 10$ mm, and: (a) $D = 10$ mm, (b) $D = 20$ mm, (c) $D = 40$ mm

step locations of 20 mm and 40 mm, clockwise recirculation patterns are observed besides the counterclockwise vortex, as shown in right side of Figs. 14b and 14c.

The strength of the counterclockwise vortex decreases with an increase in the separation distance. It is clear from Fig. 14 that at $D = 10$ mm, a counterclockwise vortex supports the transport of fuel towards the step and a clockwise vortex transports the fuel in the case of $D = 40$ mm. Oxygen penetrations are quite similar by observing its mass fraction lines of 0.16 and 0.23. However, the contour line of 0.02 shows notable differences with respect to its positioning. Clearly, as the step location increases, the contour line of oxygen mass fraction of 0.02 shifts away from the leading edge of the fuel injector.

4. Conclusions

Numerical simulations of flow features behind backward facing steps of different configurations are presented systematically. Details of flow, species and temperature fields, which help in improving the understanding of flame structure and flame anchoring, have been presented.

From a single clockwise vortex observed behind the backward facing step in the case of single fluid flow, the flow field changes to exhibit complex patterns with multiple vortices and curved flow paths for reactive flow behind the step. Based on the geometry and location of the backward facing step, several flame configuration and stability characteristics are obtained. The transition of the flame from plate to step stabilized regime is caused by an increase in air inertia forming a strong wake region behind the step.

As the height of the step is increased, oxygen flow into the wake region decreases causing the formation of a step stabilized flames. A small counterclockwise and S-shaped flow field present in the case of a plate stabilized flame changes to a counterclockwise vortex in step stabilized case. For smaller step height of 5 mm, a clockwise vortex changes to a clockwise vortex with S-shaped flow. A variation in the step location leads to significant changes in the flow behind the step. It can be concluded that the clockwise vortex at larger step locations is responsible for the enhanced flame stability.

These results are quite useful in understanding the effects of step height, step location and air velocity on resultant flow fields responsible for flame anchoring.

Acknowledgements

The authors thank P.G. Senapathy centre for computing resources, IIT Madras, for providing the computational facility required for the present work.

References

- [1] D. Andriani, A. Wresta, T.D. Atmaja, and A. Saepudin. A review on optimization production and upgrading biogas through CO₂ removal using various techniques. *Applied Biochemistry and Biotechnology*, 172(4):1909–1928, 2014. doi: [10.1007/s12010-013-0652-x](https://doi.org/10.1007/s12010-013-0652-x).
- [2] I.U. Khan, Mohd H.D. Othman, H. Hashim, T. Matsuura, A.F. Ismail, M. Rezaei-DashtArzhandi, and I. Wan Azelee. Biogas as a renewable energy fuel – A review of biogas upgrading utilization and storage. *Energy Conversion and Management*, 150:277–294, 2017. doi: [10.1016/j.enconman.2017.08.035](https://doi.org/10.1016/j.enconman.2017.08.035).
- [3] S. Rasi, A. Veijanen, and J. Rintala. Trace compounds of biogas from different biogas production plants. *Energy*, 32(8):1375–1380, 2007. doi: [10.1016/j.energy.2006.10.018](https://doi.org/10.1016/j.energy.2006.10.018).
- [4] E. Ryckebosh, M. Drouillon, and H. Vervaeren. Techniques for transformation of biogas to biomethane. *Biomass and Bioenergy*, 35(5):1633–1645, 2011. doi: [10.1016/j.biombioe.2011.02.033](https://doi.org/10.1016/j.biombioe.2011.02.033).
- [5] R.J. Spiegel, and J.L. Preston. Test results for fuel cell operation on anaerobic digester gas. *Journal of Power Sources*, 86(1-2):283–288, 2000. doi: [10.1016/S0378-7753\(99\)00461-9](https://doi.org/10.1016/S0378-7753(99)00461-9).
- [6] H.-C. Shin, J.-W. Park, K. Park, and H.-C. Song. Removal characteristics of trace compounds of landfill gas by activated carbon adsorption. *Environmental Pollution*, 119(2):227–236, 2002. doi: [10.1016/S0269-7491\(01\)00331-1](https://doi.org/10.1016/S0269-7491(01)00331-1).
- [7] R.J. Spiegel and J.L. Preston. Technical assessment of fuel cell operation on anaerobic digester gas at the Yonkers, NY, wastewater treatment plant. *Waste Management*, 23(8):709–717, 2003. doi: [10.1016/S0956-053X\(02\)00165-4](https://doi.org/10.1016/S0956-053X(02)00165-4).
- [8] A. Lock, S.K. Aggarwal, I.K. Puri, and U. Hegde. Suppression of fuel and air stream diluted methane-air partially premixed flames in normal and microgravity. *Fire Safety Journal*, 43(1):24–35, 2008. doi: [10.1016/j.firesaf.2007.02.004](https://doi.org/10.1016/j.firesaf.2007.02.004).
- [9] T. Leung and I. Wierzbna. The effect of hydrogen addition on biogas non-premixed jet flame stability in a co-flowing air stream. *International Journal of Hydrogen Energy*, 33(14):3856–3862, 2008. doi: [10.1016/j.ijhydene.2008.04.030](https://doi.org/10.1016/j.ijhydene.2008.04.030).
- [10] A.M. Briones, S.K. Aggarwal, and V. Katta. A numerical investigation of flame liftoff, stabilization, and blowout. *Physics of Fluids*, 18(4):043603, 2006. doi: [10.1063/1.2191851](https://doi.org/10.1063/1.2191851).
- [11] C.-E. Lee and C.-H. Hwang. An experimental study on the flame stability of LFG and LFG-mixed fuels. *Fuel*, 86(5-6):649–655, 2007. doi: [10.1016/j.fuel.2006.08.033](https://doi.org/10.1016/j.fuel.2006.08.033).
- [12] L. Xiang, H. Chu, F. Ren, and M. Gu. Numerical analysis of the effect of CO₂ on combustion characteristics of laminar premixed methane/air flames. *Journal of the Energy Institute*, 92(5):1487–1501, 2019. doi: [10.1016/j.joei.2018.06.018](https://doi.org/10.1016/j.joei.2018.06.018).
- [13] N. Hinton and R. Stone. Laminar burning velocity measurements of methane and carbon dioxide mixtures (biogas) over wide ranging temperatures and pressures. *Fuel*, 116:743–750, 2014. doi: [10.1016/j.fuel.2013.08.069](https://doi.org/10.1016/j.fuel.2013.08.069).
- [14] S. Jahangirian, A. Engeda, and I.S. Wichman. Thermal and chemical structure of biogas counterflow diffusion flames. *Energy and Fuels*, 23(11):5312–5321, 2009. doi: [10.1021/ef9002044](https://doi.org/10.1021/ef9002044).
- [15] A. Mameri and F. Tabet. Numerical investigation of counter-flow diffusion flame of biogas-hydrogen blends: Effects of biogas composition, hydrogen enrichment and scalar dissipation rate on flame structure and emissions. *International Journal of Hydrogen Energy*, 41(3):2011–2022, 2016. doi: [10.1016/j.ijhydene.2015.11.035](https://doi.org/10.1016/j.ijhydene.2015.11.035).
- [16] J.I. Erete, K.J. Hughes, L. Ma, M. Fairweather, M. Pourkashanian, and A. Williams. Effect of CO₂ dilution on the structure and emissions from turbulent, non-premixed methane-air jet flames. *Journal of the Energy Institute*, 90(2):191–200, 2017. doi: [10.1016/j.joei.2016.02.004](https://doi.org/10.1016/j.joei.2016.02.004).
- [17] M.R.J. Charest, Ö.L. Gülder, and C.P.T. Groth. Numerical and experimental study of soot formation in laminar diffusion flames burning simulated biogas fuels at elevated pressures. *Combustion and Flame*, 161(10):2678–2691, 2014. doi: [10.1016/j.combustflame.2014.04.012](https://doi.org/10.1016/j.combustflame.2014.04.012).

- [18] H.M. Nicholson and J.P. Field. Some experimental techniques for the investigation of the mechanism of the flame stabilization in the wakes of bluff bodies. *Symposium on Combustion and Flame, and Explosion Phenomena*, 3(1):44–68, 1948. doi: [10.1016/S1062-2896\(49\)0008-0](https://doi.org/10.1016/S1062-2896(49)0008-0).
- [19] G.C. Williams and C.W. Shipman. Some properties of rod-stabilized flames C homogenous gas mixtures. *Symposium (International) on Combustion*, 4(1):733-742, 1953. doi: [10.1016/S0082-0784\(53\)80096-2](https://doi.org/10.1016/S0082-0784(53)80096-2).
- [20] G.C. Williams, P.T. Woo, and C.W. Shipman. Boundary layer effects on stability characteristics of bluff-body flame holders. *Symposium (International) on Combustion*, 6(1):427–438, 1957. doi: [10.1016/S0082-0784\(57\)80058-7](https://doi.org/10.1016/S0082-0784(57)80058-7).
- [21] E.E. Zukoski, and F.E. Marble. Experimental concerning the mechanism of flame blowoff from bluff bodies. *Proceedings of the Gas Dynamics Symposium on Aerothermochemistry*, 205-210, 1956.
- [22] E.E. Zukoski. Flame stabilization on bluff bodies at low and intermediate Reynolds numbers. Ph.D Thesis, California Institute of Technology, Pasadena, United States of America, 1954. doi: [10.7907/E9V0-GM76](https://doi.org/10.7907/E9V0-GM76).
- [23] T. Maxworthy. On the mechanism of bluff body flame stabilization at low velocities. *Combustion and Flame*, 6:233–244, 1962. doi: [10.1016/0010-2180\(62\)90101-3](https://doi.org/10.1016/0010-2180(62)90101-3).
- [24] S.I. Cheng and A.A. Kovitz. Theory of flame stabilization by a bluff body. *Symposium (International) on Combustion*, 7(1):681–691, 1958. doi: [10.1016/S0082-0784\(58\)80109-5](https://doi.org/10.1016/S0082-0784(58)80109-5).
- [25] A.A. Kovitz and H.-M Fu. On bluff body flame stabilization. *Applied Scientific Research*, 10:315–334, 1961. doi: [10.1007/BF00411927](https://doi.org/10.1007/BF00411927).
- [26] C.-H. Chen and J.S. T'ien. Diffusion flame stabilization at the leading edge of fuel plate. *Combustion Science and Technology*, 50(4-6):283–306, 1986. doi: [10.1080/00102208608923938](https://doi.org/10.1080/00102208608923938).
- [27] T. Rohmat, H. Katoh, T. Obara, T. Yoshihashi, and S. Ohyagi. Diffusion flame stabilized on a porous plate in a parallel airstream. *AIAA Journal*, 36(11):1945–1952, 1998. doi: [10.2514/2.300](https://doi.org/10.2514/2.300).
- [28] E.D. Gopalakrishnan and V. Raghavan. Numerical investigation of laminar diffusion flames established on a horizontal flat plate in a parallel air stream. *International Journal of Spray and Combustion Dynamics*, 3(2):161–190, 2011. doi: [10.1260/1756-8277.3.2.161](https://doi.org/10.1260/1756-8277.3.2.161).
- [29] P.K. Shijin, S. Soma Sundaram, V. Raghavan, and V. Babu. Numerical investigation of laminar cross flow non-premixed flames in the presence of a bluff-body. *Combustion Theory and Modelling*, 18(6):692–710, 2014. doi: [10.1080/13647830.2014.967725](https://doi.org/10.1080/13647830.2014.967725).
- [30] P.K. Shijin, V. Raghavan, and V. Babu. Numerical investigation of flame-vortex interactions in cross flow non-premixed flames in the presence of bluff bodies. *Combustion Theory and Modelling*, 20(4):683–706, 2016. doi: [10.1080/13647830.2016.1168942](https://doi.org/10.1080/13647830.2016.1168942).
- [31] P.K. Shijin, A. Babu, and V. Raghavan. Experimental study of bluff body stabilized laminar reactive boundary layers. *International Journal of Heat and Mass Transfer*, 102:219–225, 2016. doi: [10.1016/j.ijheatmasstransfer.2016.06.028](https://doi.org/10.1016/j.ijheatmasstransfer.2016.06.028).
- [32] A. Harish, H.R. Rakesh Ranga, A. Babu, and V. Raghavan. Experimental study of the flame characteristics and stability regimes of biogas-air cross flow non-premixed flames. *Fuel*, 223:334–343, 2018. doi: [10.1016/j.fuel.2018.03.055](https://doi.org/10.1016/j.fuel.2018.03.055).
- [33] R.A. Barlow, A.N. Karpetis, J.H. Frank, and J.-Y Chen. Scalar profiles and NO formation in laminar opposed-flow partially premixed methane/air flames. *Combustion and Flame*, 127(3):2102–2118, 2001. doi: [10.1016/S0010-2180\(01\)00313-3](https://doi.org/10.1016/S0010-2180(01)00313-3).
- [34] T. Hirano and Y. Kanno. Aerodynamics and thermal structures of the laminar boundary layer over a flat plate with a diffusion flame. *Symposium (International) on Combustion*, 14(1):391–398, 1973. doi: [10.1016/S0082-0784\(73\)80038-4](https://doi.org/10.1016/S0082-0784(73)80038-4).